

Non-universal SUGRA at LHC: Prospects and Discovery Potential

Subhaditya Bhattacharya¹, Shreyashi Chakdar², Kirtiman Ghosh³, S. Nandi⁴

1. Department of Physics and Astronomy,
University Of California, Riverside, CA 92501, USA

2,3,4. Department of Physics, Oklahoma State University, and Oklahoma Center for High
Energy Physics, Stillwater, OK 74078, USA

Abstract

We explore supersymmetry (SUSY) parameter space with non-universal high scale parameters in gravity mediated SUSY breaking (SUGRA) scenario that accommodates a Higgs mass of (125 ± 2) GeV while satisfying cold dark matter relic density and other low energy constraints. We indicate a few benchmark points consistent with different dark matter annihilation processes where third family squarks are lighter than the first two as a requirement to keep the Higgs mass within the limit. We show that bottom rich and leptonic final states have better reach in such parameter space points and is the most likely scenario to discover SUSY at the upcoming run of LHC with center-of-mass energy 14 TeV.

¹E-mail: subhaditya123@gmail.com

²E-mail: chakdar@okstate.edu

³E-mail: kirti.gh@gmail.com

⁴E-mail: s.nandi@okstate.edu

1 Introduction

Supersymmetry (SUSY) [1, 2] has been under scanner since last forty years or more. Ongoing Large Hadron Collider (LHC) has put strong bounds on the squark and gluino masses of minimal supersymmetric Standard Model (MSSM); particularly on minimal supergravity (mSUGRA) or constrained minimal supersymmetric Standard Model (CMSSM) [3], not seeing any of those supersymmetric particles. Still, SUSY search in different forms is the most studied subject of particle physics research due to its unparalleled theoretical appeal and phenomenological implications.

Out of different SUSY-breaking schemes, mSUGRA has been most popular due to its economy of parameters; the universal gaugino mass ($M_{1/2}$), the universal scalar mass (m_0), the universal trilinear coupling (A_0) all at the GUT scale, $\tan\beta$, the ratio of the vacuum expectation values (vev) of the two Higgses and the sign of SUSY-conserving Higgsino mass parameter μ . However, this framework has been highly constrained by direct and indirect search experiments [4–7] and non-universality in scalar [8–19] and gaugino masses [20–22] are getting more and more importance to keep low-scale SUSY alive.

Recent discovery of Higgs boson with $m_H \simeq 125$ GeV at LHC by the ATLAS and CMS Collaborations [23] has put a severe constraint on SUSY parameter space. SUSY Higgs gets significant correction from the top squark (stop) loop, which increases with increasing stop mixing and/or stop mass scale. Therefore, in order to get a Higgs boson around 125 GeV, significant stop mixing or a large stop mass scale is required. Large stop mixing results into large mass splitting in the stop sector and consequently gives rise to a lighter stop (\tilde{t}_1) in the mass spectrum. Hence, Higgs boson mass at 125 GeV results in a SUSY mass spectrum with light third family scalars.

Light third family scalars, but relatively heavy first two families¹ favor SUSY discovery at future LHC runs given gluino (\tilde{g}) dominantly decays into top-stop pairs ($\tilde{g} \rightarrow t\tilde{t}_1$) and subsequently stop decays into top-neutralino or b-chargino where $t \rightarrow bW^\pm$ gives rise to multiple b-jets, leptons and large missing energy ($E_{\cancel{T}}$). Final states with multiple b jets and charged leptons, together with large missing energy, cut down the SM background much more than the usual SUSY signals with multijets plus large missing energy, and both ATLAS and CMS experiments has achieved b-tagging efficiency 50% or more and have put bounds on SUSY from the available data [5].

Another important aspect of SUSY is the dark matter (DM); R -parity conservation yields

¹Such scenarios have already been considered for studies in different contexts [8–10].

a natural candidate namely, the lightest supersymmetric particle (LSP). DM relic density limits from WMAP [24] and PLANCK [25] can be easily satisfied in the non-universal gaugino and/or scalar mass scenarios where CMSSM is tightly constrained. For example, if wino mass is smaller than bino mass at GUT scale ($M_2 \leq M_1$), we obtain wino dominated LSP yielding correct abundance in a larger parameter space. Similarly, non-universality in the scalar sector may result in a higgsino like LSP (from non-universality in the Higgs sector) or stau-LSP co annihilation (from non-universality in the soft SUSY breaking stau mass). We have systematically studied such non-universal gaugino and/or scalar mass scenarios and proposed benchmark points for collider studies at LHC with $E_{CM} = 14$ TeV.

Vast amount of work has already been done in mSUGRA to discover SUSY at the LHC. However, because of the observed Higgs mass, and the dark matter constraint, the only region left in mSUGRA and accessible at the LHC is the stop co-annihilation region (where the lighter top squark \tilde{t}_1 and the lightest neutralino $\tilde{\chi}_1^0$ annihilate to satisfy the dark matter constraint. However, in this parameter space, \tilde{t}_1 mass is very close to the $\tilde{\chi}_1^0$ mass giving rise to very little high p_T multijet activity from its decay [26]. Significant number of works have also been done by increasing the number of parameters, with non-universal gaugino masses and non-universality in the scalar masses satisfying all the existing constraints [27]. However, we pin point that to survive Higgs mass and dark matter constraint in the framework of gravity mediated supersymmetry breaking, a larger region of parameter space is available with specific non-universal gaugino and scalar mass patterns with a generic signature in bottom rich, and bottom quark plus charged lepton rich final states with large missing energy, which with suitable cuts can be observed over the SM background at the 14 TeV LHC. We claim that these will be the most favorable final states at the 14 TeV LHC to discover SUSY or to put strongest bounds on them.

The paper is organized as follows. In Section 2, we discuss the model under consideration and the selected benchmark points. We also review dark matter constraints on SUSY parameter space to motivate our benchmark points. In Section 3, we discuss the final states in which SUSY signals can be observed over the SM background, including the details of the collider simulation strategy and the numerical results at the 14 TeV LHC. We conclude in Section 4.

2 Model, Constraints and Benchmark Points

2.1 Constraints on SUSY models:

Following measurements play a key role to constrain SUSY parameter space. We discuss their effect and motivate how that leads eventually to the benchmark points chosen in this article for SUSY searches at LHC.

- The main constraint on the SUSY parameter space after LHC 7/8 TeV data is that the CP even Higgs mass to be within [23]:

$$123 \leq m_h \leq 127. \quad (1)$$

- The branching ratio for $b \rightarrow s\gamma$ [6] which at the 3σ level is

$$2.13 \times 10^{-4} < Br(b \rightarrow s\gamma) < 4.97 \times 10^{-4}. \quad (2)$$

- We also take into account the constraint coming from $B_s \rightarrow \mu^+\mu^-$ branching ratio which by LHCb observation [7] at 95% CL is given as

$$2 \times 10^{-9} < Br(B_s \rightarrow \mu^+\mu^-) < 4.7 \times 10^{-9}. \quad (3)$$

- Parameters are fine-tuned in a way that it gives a correct cold dark matter relic abundance according to WMAP data [24], which at 3σ is

$$0.091 < \Omega_{CDM}h^2 < 0.128, \quad (4)$$

where Ω_{CDM} is the dark matter relic density in units of the critical density and $h = 0.71 \pm 0.026$ is the reduced Hubble constant (namely, in units of $100 \text{ km s}^{-1} \text{ Mpc}^{-1}$).

To note here, the PLANCK constraints $0.112 \leq \Omega_{DM}h^2 \leq 0.128$ [25] is more stringent, and cuts a significant amount of dark matter allowed SUSY parameter space. We choose our benchmark points satisfying PLANCK on top of WMAP.

In the following subsection, we discuss mainly the dark matter and Higgs mass constraints on SUSY parameter space as they have been the key to choose our benchmark points.

2.2 Dark matter and Higgs mass on SUSY: Benchmark Points

One of the main motivations for postulating R -parity conserving SUSY is the presence of a stable weakly interacting massive particle (WIMP) which can be a good cold dark matter. Lightest neutralino $\tilde{\chi}_1^0$ is most often the lightest supersymmetric particle (LSP) and a good candidate for cold dark matter. In some regions of the parameter space, it has the annihilation cross-section to Standard Model (SM) particles yielding correct relic abundance satisfying WMAP/PLANCK [24, 25].

In mSUGRA, $\tilde{\chi}_1^0$ is bino dominated in a large part of the parameter space. For a bino DM, WIMP miracle occurs when they annihilate to leptons via t -channel exchange of sleptons with mass in the 30-80 GeV range [28]. However, slepton masses that light was already discarded by direct slepton searches at LEP2 [29]. Therefore, after LEP2, some distinct parts of mSUGRA parameter space that satisfies relic abundance are as follows:

- **The h -resonance region** [30] is characterized by $2m_{\tilde{\chi}_1^0} \sim m_h$ which occurs at low $m_{1/2}$. In this region, $\tilde{\chi}_1^0$ annihilation cross-section enhances due to the presence of a s -channel h -resonance.
- **A -funnel region** [31] is where $2m_{\tilde{\chi}_1^0} \sim m_A$; A is the CP-odd Higgs boson. This region is characterized by large $\tan\beta \sim 50$.
- **Hyperbolic branch/focus point (HB/FP) region** [32] is the parameter space where large m_0 region corresponds to small μ and thus Higgsino dominates $\tilde{\chi}_1^0$ and annihilates to WW , ZZ and Ah significantly.
- **Stau co-annihilation region** [33] arises if neutralino-LSP is nearly degenerate with the stau ($m_{\tilde{\chi}_1^0} \simeq m_{\tilde{\tau}_1}$). In mSUGRA, this occurs at low m_0 and high $M_{1/2}$.
- **Stop co-annihilation** [34] occurs in mSUGRA with some particular values of A_0 , where lighter stop (\tilde{t}_1) becomes nearly degenerate with the LSP.

After LHC data with the discovery of Higgs and exclusion limits on the squark/gluino masses, many of the above DM regions in mSUGRA are highly constrained. With 20.3 fb^{-1} integrated luminosity and $E_{CM} = 8 \text{ TeV}$, ATLAS [35] and CMS [36] collaborations have excluded equal squark and gluino mass below 1.7 TeV completely ruling out h -resonance region whereas, the A -funnel, stau and stop co-annihilation regions are partly excluded. Observation of Higgs mass at about 125 GeV indicates towards large m_0 ($m_0 > 0.8 \text{ TeV}$) and large A_0 ($|A_0| > 1.8m_0$ for $m_0 < 5 \text{ TeV}$) [37]. For $m_0 > 0.8 \text{ TeV}$, stau co-annihilation

is only viable at very large $M_{1/2}$ values which makes the SUSY discovery at the collider very challenging. The HB/FP region remains unscathed by the LHC squark/gluino searches as it requires low μ at very large $m_0 \sim 3 - 10$ TeV for $A_0 = 0$. However, Higgs mass at 125 GeV (requires large $|A_0|$) push the region to much higher $m_0 \sim 10 - 50$ TeV values. A small part of stop co-annihilation is the only region of mSUGRA parameter space alive, having some possibilities of seeing at 14 TeV LHC.

Non-universality in the gaugino and/or scalar sector on the other hand, can provide a lot more breathing space. The implications of direct search bound from LHC on neutralino dark matter have been studied extensively. See for example, [38–40]. In our analysis, we choose four benchmark points (BP) which are motivated from different LSP annihilation and co-annihilation mechanism and consistent with all experimental limits.

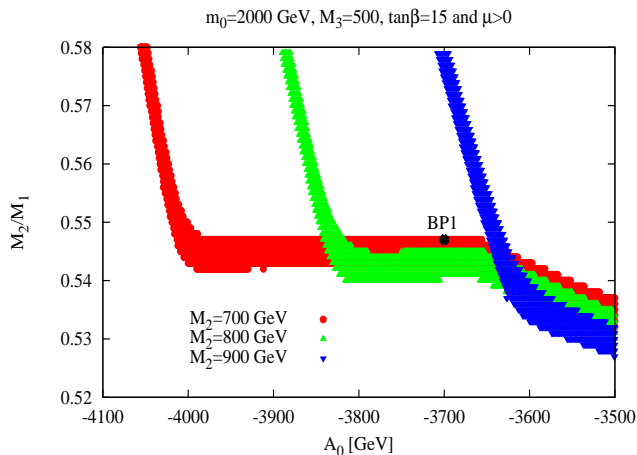


Figure 1: A sample parameter space scan for gaugino mass non-universality with $M_3 < M_2 < M_1$ in A_0 vs M_2/M_1 plane to satisfy DM abundance. $M_2 = (700, 800, 900)$ GeV, yields three discrete consistent regions in red, blue and green respectively with M_2/M_1 varying along y-axis with A_0 varying along x-axis. We choose $M_3 = 500$ GeV, $m_0 = 2000$ GeV, $\tan \beta = 15$. BP1 represent a benchmark point of this sort.

i) BP1: If $M_2 < M_1$ at GUT scale and EW scale, and $M_2 < \mu$ at low scale, the LSP $\tilde{\chi}_1^0$ is wino dominated and then lightest chargino is almost degenerate with LSP. Chargino co-annihilation crucially controls relic abundance in such a region of parameter space, apart from larger wino component itself increases annihilation cross-section. A large part of purely wino

DM hence provides under-abundance [41]. However, we scan the wino dominated parameter space where it is consistent with relic abundance from WMAP. As an example, we have scanned the parameter space over M_1 , M_2 and A_0 for $m_0 = 2000$ GeV, $M_3 = 500$ GeV $\tan\beta = 15$ and $\mu > 0$. The allowed values of M_2/M_1 as a function of A_0 are plotted in Fig. 1 for three different values $M_2 = 700, 800$ and 900 GeV in red, blue and green respectively. When we vary M_2 continuously, they merge into a continuous region. It is important to note in Fig. 1 the vertical high A_0 region is dominated by stop co annihilation as the stop becomes lighter with increasing A_0 and a small change in A_0 results in a big change in M_2/M_1 to keep relic abundance within proper limit. The horizontal part of red, blue and green region with smaller A_0 on the other hand, represent wino dominated dark matter with nearly degenerate chargino and co-annihilation to yield proper abundance. For example, with $M_2 = 700$ GeV, $|A_0| > 4000$ GeV is dominated by stop co-annihilation and $|A_0| < 4000$ GeV characterizes wino DM. Our first benchmark point BP1 is a representative of this particular non-universal gaugino mass scenario $M_3 < M_2 < M_1$ with wino dominated DM. The benchmark points are explicitly written in Table 2. While gaugino mass non-universality has been used to obtain BP1, scalar masses are kept universal.

Also note that gaugino non-universality with $M_3 < M_2 < M_1$ is obtained within the framework of SUSY-GUT in $SU(5)$ or $SO(10)$ [20, 21] with dimension five operator in the extension of the gauge kinetic function $f_{\alpha\beta}(\Phi^j)$

$$Re f_{\alpha\beta}(\phi) F_{\mu\nu}^\alpha F^{\beta\mu\nu} = \frac{\eta(\Phi^s)}{M} Tr(F_{\mu\nu} \Phi^N F^{\mu\nu}) \quad (5)$$

where non-singlet chiral superfields Φ^N belongs to the symmetric product of the adjoint representation of the underlying gauge group as

$$\begin{aligned} SU(5) : \quad (24 \times 24)_{symm} &= 1 + 24 + 75 + 200 \\ SO(10) : \quad (45 \times 45)_{symm} &= 1 + 54 + 210 + 770 \end{aligned} \quad (6)$$

Gaugino masses become non-universal if these non-singlet Higgses are responsible for the GUT-breaking. 75 and 200 belonging to $SU(5)$ or 770^2 of $SO(10)$ yield a hierarchy of $M_3 < M_1, M_2$ shown in Table 1. The specific non-universal ratio(s) used in the scan can be motivated from GUT breaking with a linear combination of aforementioned non-singlet representations.

²For breaking through 770, we quote the result, when it breaks through the Pati-Salam gauge group $G_{422D} (SU(4)_C \times SU(2)_L \times SU(2)_R$ with even D-parity and assumed to break at the GUT scale itself.

| Representation | $M_3 : M_2 : M_1$ at M_{GUT} |
|--|--------------------------------|
| 75 of $SU(5)$ | 1:3:(-5) |
| 200 of $SU(5)$ | 1:2:10 |
| 770 of $SO(10)$: $H \rightarrow SU(4) \times SU(2) \times SU(2)$ | 1:(2.5):(1.9) |

Table 1: Non-universal gaugino mass ratios for different non-singlet representations belonging to $SU(5)$ or $SO(10)$ GUT-group that gives rise to the hierarchy of $M_3 < M_1, M_2$ at the GUT scale.

ii) BP2: Our second benchmark point BP2 is motivated from the Hyperbolic branch/Focus Point region of DM. As has already been mentioned, for mSUGRA, very large values $m_0 \sim 10 - 50$ TeV is required to make μ small such that LSP becomes predominantly a Higgsino, that paves the way for correct relic abundance through annihilation to WW , ZZ and Ah final states. However, introduction of non-universality in the scalar sector, in particular in the Higgs parameters m_{H_u} and m_{H_d} at GUT scale, gives rise to small μ , even without going to such high scalar masses, making it accessible to collider events at LHC. Again, following our strategy to minimize the number of parameters to choose BP2, we kept all gaugino and other scalar masses universal at the high scale.

iii) BP3: Our third benchmark point BP3 represents stau co-annihilation region exploiting non-universality in the scalar sector. We have used squark-slepton non-universality as well as non-universality in the family to make the third family slepton masses lighter than other scalars at the high scale. Although such scalar non-universality is mostly phenomenological, having impacts on CP and FCNC issues, it can be motivated from string-inspired models with flavor dependent couplings to the modular fields [8,9]. In Table 2 we show all the inputs at high scale as well as the low-scale SUSY masses.

iv) MSG: The mSUGRA benchmark point represent stop co-annihilation region of DM parameter space. In mSUGRA, stop co-annihilation occurs at distinct non-zero values of $|A_0|$ in a narrow range, for particular values of m_0 , $M_{1/2}$, $\tan\beta$ and $\text{Sign}(\mu)$. Higgs mass of 125 GeV can also be obtained in the whole $m_0 - M_{1/2}$ plane with $m_0 > 0.8$ TeV for large A_0 . Hence, a tiny region of m_0 , $M_{1/2}$ and A_0 parameter space simultaneously satisfy right Higgs mass and dark matter constraints.

However, the situation changes dramatically if we introduce non-universality in gaugino sector, if we assume $M_3 < M_2 = M_1$, effectively adding one more parameter to mSUGRA.

Then Higgs mass of 125 GeV can be satisfied in a larger range of A_0 values; while for a given A_0 , dark matter density can be satisfied by varying $M_{1,2}$ appropriately through stop co-annihilation.

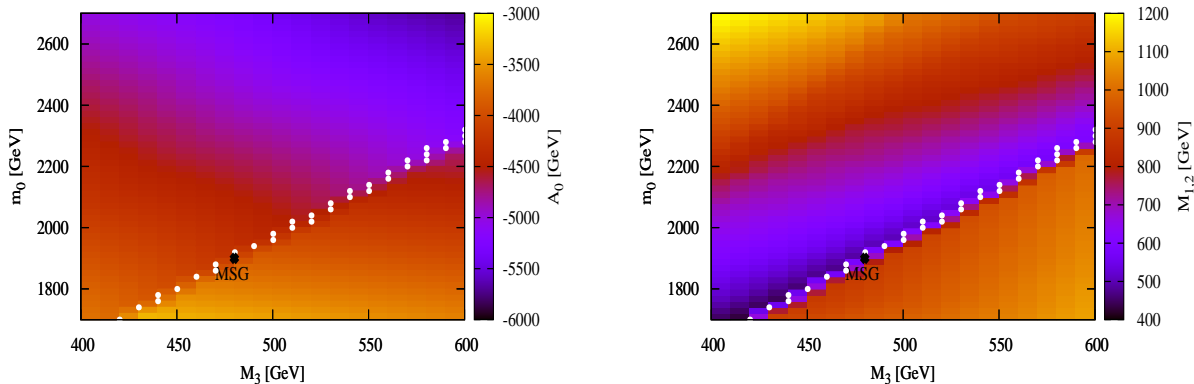


Figure 2: Four-dimensional parameter space scan with m_0 , M_3 , $M_{1,2}$ and A_0 ; for $\tan\beta = 15$ and positive μ to obtain correct dark matter relic abundance, Higgs mass and other low energy constraints. LHS: Three-dimensional subset of the scan with M_3 (along x-axis), m_0 (along y-axis), A_0 (color gradient); RHS: M_3 (along x-axis), m_0 (along y-axis) and $M_{1,2}$ (color gradient). mSUGRA points are represented in white dots and our benchmark MSG is one of them.

In Fig. 2, we have presented a sample scan of such a four-dimensional parameter space m_0 , M_3 , $M_{1,2}$ and A_0 , for $\tan\beta = 15$ and positive μ . Left panel shows a three-dimensional subset of the scan with M_3 (along x-axis), m_0 (along y-axis), A_0 (color gradient) and on the right panel we have M_3 (along x-axis), m_0 (along y-axis) and $M_{1,2}$ (color gradient). For a given M_3 and m_0 , there is a range of A_0 and $M_{1,2}$ which gives rise to right relic abundance and Higgs mass. For simplicity, in Fig. 2, we consider the minimum possible values of A_0 and $M_{1,2}$ which are consistent with experimental constraints. As a result, the whole parameter space shown in the figure is allowed by dark matter and Higgs mass constraint. White dots in Fig. 2 corresponds to $M_3 = M_{1,2}$, i.e. mSUGRA points as a subspace of such gaugino non-universality. Our benchmark point MSG is represented by one of these white dots. We didn't chose a non-universal benchmark point from this region as the collider signature is

expected to be the same as the chosen MSG point.

For renormalization group equation RGE, we use the code `SuSpect v2.3` [42] with $m_t = 173.2$ GeV, $m_b = 4.2$ GeV, $m_\tau = 1.777$ GeV and stick to two-loop RGE with radiative corrections to the gauginos and squarks. We use full one loop and dominant two loop corrections for the Higgs mass. We ensure radiative electroweak symmetry breaking to evaluate the Higgsino parameter μ at the low scale out of high-scale inputs $m_{H_u}^2$ and $m_{H_d}^2$ and the electroweak symmetry breaking scale has been set at $\sqrt{m_{\tilde{t}_L} m_{\tilde{t}_R}}$, the default value in the code `SuSpect`. The low scale value of the strong coupling constant has been chosen at $\alpha_3(M_Z)^{\overline{MS}} = 0.1172$. We compute the cold dark matter relic density with the code `micrOMEGAs3.1` [43].

3 Collider Simulation and Results

Non-universal SUGRA points advocated in the earlier section can be seen at the future run of LHC in bottom rich and leptonic final states. This also serves as a major distinguishing feature from mSUGRA points surviving Higgs mass and dark matter constraints.

We first discuss the strategy for the simulation including the final state observables and the cuts employed therein and then we discuss the numerical results in next subsection.

3.1 Strategy for Simulation

The spectrum generated by `SuSpect` as described in the earlier section, at the benchmark points are fed into the event generator `Pythia 6.4.16` [44] by `SLHA` interface [45] for the simulation of pp collision with centre of mass energy 14 TeV for LHC.

The default parton distribution functions `CTEQ5L` [46], QCD scale $\sqrt{\hat{s}}$ in `Pythia` has been used. All possible SUSY processes (mainly 2→2) and decay chains consistent with conserved R -parity have been kept open with initial and final state radiation on. We take hadronization into account using the fragmentation functions inbuilt in `Pythia`.

The main 'physics objects' that are reconstructed in a collider, are:

- Isolated leptons identified from electrons and muons
- Hadronic Jets formed after identifying isolated leptons
- Unclustered Energy made of calorimeter clusters with $p_T > 0.5$ GeV (ATLAS) and $|\eta| < 5$, not associated to any of the above types of high- E_T objects (jets or isolated

| parameter | BP1 | BP2 | BP3 | MSG |
|-------------------------------------|-----------------------|-----------------------|-----------------------|-----------------------|
| $\tan \beta$ | 15.00 | 15.00 | 15.00 | 15.00 |
| (M_3, M_2, M_1) | (500,700,1282) | (500,500,500) | (500,500,500) | (480,480,480) |
| $(m_{\tilde{f}}, m_{\tilde{\tau}})$ | (2000,2000) | (2500,2500) | (2000,518) | (1900,1900) |
| (m_{H_u}, m_{H_d}) | (2000,2000) | (3047,4000) | (2000,2000) | (1900,1900) |
| A_0 | -3700 | -3500 | -3500 | -4239 |
| $sgn(\mu)$ | + | + | + | + |
| $m_{\tilde{g}}$ | 1251 | 1277 | 1265.2 | 1201.3 |
| $m_{\tilde{u}_L}$ | 2234 | 2667 | 2217.6 | 2108 |
| $m_{\tilde{t}_1}$ | 761 | 785.6 | 865 | 243 |
| $m_{\tilde{t}_2}$ | 1656.5 | 1950.2 | 1670 | 1487 |
| $m_{\tilde{b}_1}$ | 1635 | 1940.5 | 1651 | 1442 |
| $m_{\tilde{b}_2}$ | 2117 | 2558.3 | 2124.6 | 1988 |
| $m_{\tilde{e}_L}$ | 2054 | 2473 | 2019 | 1918.3 |
| $m_{\tilde{\tau}_1}$ | 1962 | 2420.3 | 219.7 | 1797 |
| $m_{\tilde{\tau}_2}$ | 2013.8 | 2467.2 | 492.2 | 1870 |
| $m_{\tilde{\chi}_1^\pm}$ | 588.3 | 262.6 | 417.6 | 404.6 |
| $m_{\tilde{\chi}_2^\pm}$ | 1584.4 | 447.5 | 1523 | 1742 |
| $m_{\tilde{\chi}_4^0}$ | 1584.3 | 447.7 | 1522.4 | 1741 |
| $m_{\tilde{\chi}_3^0}$ | 1581.3 | 285.3 | 1520.3 | 1739.4 |
| $m_{\tilde{\chi}_2^0}$ | 588.4 | 275.3 | 417.6 | 404.6 |
| $m_{\tilde{\chi}_1^0}$ | 561.7 | 201.7 | 211.4 | 208.3 |
| m_h | 124.1 | 123.4 | 123.2 | 123.8 |
| $\Omega_{\tilde{\chi}_1} h^2$ | 0.118 | 0.127 | 0.116 | 0.112 |
| $BF(b \rightarrow s\gamma)$ | 2.98×10^{-4} | 2.83×10^{-4} | 3.00×10^{-4} | 3.25×10^{-4} |
| $Br(B_s \rightarrow \mu^+ \mu^-)$ | 3.10×10^{-9} | 3.07×10^{-9} | 3.09×10^{-9} | 3.13×10^{-9} |

Table 2: Benchmark points BP1, BP2, BP3 and MSG. Model inputs, low scale predictions (Masses in GeV) and values of the constraints including Higgs mass and relic density are mentioned.

leptons).

We try to mimic the experimental reconstruction for these objects in Pythia as follows.

- Isolated leptons (ℓ):

Isolated leptons are identified as electrons and muons with $p_T > 10$ GeV and $|\eta| < 2.5$. An isolated lepton is separated from another lepton by $\Delta R_{\ell\ell} \geq 0.2$, from jet (jets with $E_T > 20$ GeV) with $\Delta R_{\ell j} \geq 0.4$, while the energy deposit $\sum E_T$ due to low- E_T hadron activity around a lepton within $\Delta R \leq 0.2$ of the lepton axis should be ≤ 10 GeV. $\Delta R = \sqrt{\Delta\eta^2 + \Delta\phi^2}$ is the separation in pseudo rapidity and azimuthal angle plane. The smearing functions of isolated electrons, photons and muons are described below.

- Jets (jet):

Jets are formed with all the final state particles after removing the isolated leptons from the list with PYCELL, an inbuilt cluster routine in Pythia. The detector is assumed to stretch within the pseudorapidity range $|\eta|$ from -5 to +5 and is segmented in 100 pseudorapidity (η) bins and 64 azimuthal (ϕ) bins. The minimum E_T of each cell is considered as 0.5 GeV, while the minimum E_T for a cell to act as a jet initiator is taken as 2 GeV. All the partons within $\Delta R=0.4$ from the jet initiator cell is considered for the jet formation and the minimum $\sum_{parton} E_T^{jet}$ for a collected cell to be considered as a jet is taken to be 20 GeV. We have used the smearing function and parameters for jets that are used in PYCELL in Pythia.

- b-jets:

We identify partonic b jets by simple b -tagging algorithm with efficiency of $\epsilon_b = 0.5$ for $p_T > 40$ GeV and $|\eta| < 2.5$ [47].

- Unclustered Objects ($Unc.O$):

All the other final state particles, which are not isolated leptons and separated from jets by $\Delta R \geq 0.4$ are considered as unclustered objects. This clearly means all the particles (electron/photon/muon) with $0.5 < E_T < 10$ GeV and $|\eta| < 5$ (for muon-like track $|\eta| < 2.5$) and jets with $0.5 < E_T < 20$ GeV and $|\eta| < 5$, which are detected at the detector, are considered as unclustered objects.

- Electron/Photon Energy Resolution :

$$\sigma(E)/E = a/\sqrt{E} \oplus b \oplus c/E^3 \quad (7)$$

Where,

$$\begin{array}{llll} a = 0.03 \text{ [GeV}^{1/2}\text{]}, & b = 0.005 \text{ \&} & c = 0.2 \text{ [GeV]} & \text{for } |\eta| < 1.5 \\ = 0.055 & = 0.005 & = 0.6 & \text{for } 1.5 < |\eta| < 5 \end{array}$$

- Muon P_T Resolution :

$$\sigma(P_T)/P_T = a \quad \text{if } P_T < 100\text{GeV} \quad (8)$$

$$= a + b \log(P_T/\xi) \quad \text{if } P_T > 100\text{GeV} \quad (9)$$

Where,

$$\begin{array}{llll} a = 0.008 \text{ \&} & b = 0.037 & \text{for } |\eta| < 1.5 \\ = 0.02 & = 0.05 & 1.5 < |\eta| < 2.5 \end{array}$$

and $\xi = 100 \text{ GeV}$.

- Jet Energy Resolution :

$$\sigma(E_T)/E_T = a/\sqrt{E_T} \quad (10)$$

Where,

$$a = 0.55 \text{ [GeV}^{1/2}\text{]}, \text{ default value used in PYCELL.}$$

- Unclustered Energy Resolution :

$$\sigma(E_T) = \alpha \sqrt{\sum_i E_T^{(Unc.O)i}} \quad (11)$$

Where, $\alpha \approx 0.55$. One should keep in mind that the x and y component of $E_T^{Unc.O}$ need to be smeared independently with same smearing parameter.

³ \oplus indicates addition in quadrature

We sum vectorially the x and y components of the momenta separately for all visible objects to form visible transverse momentum $(p_T)_{vis}$,

$$(p_T)_{vis} = \sqrt{(\sum p_x)^2 + (\sum p_y)^2} \quad (12)$$

where, $\sum p_x = \sum (p_x)_{iso} + \sum (p_x)_{jet} + \sum (p_x)_{Unc.O}$ and similarly for $\sum p_y$. We identify $(p_T)_{vis}$ as missing energy $E_{\cancel{H}}$:

$$E_{\cancel{H}} = (p_T)_{vis} \quad (13)$$

We also define Effective mass H_T as the scalar sum of transverse momenta of visible objects like lepton and jets with missing energy

$$H_T = \sum p_T^{\ell_i} + p_T^{jets} + E_{\cancel{H}} \quad (14)$$

Effective mass cuts have really been useful to reduce SM background for the signals as we will see shortly.

We studied the benchmark points in multi-lepton final states as well as in b-rich final states at $E_{CM} = 14$ TeV at LHC with varying cuts. The channels we study are:

- Four b-jet with inclusive lepton and jets ($4b$): $4b + X + E_{\cancel{H}}$; Here X implies any number of inclusive jets or leptons without any specific veto on that. Basic cuts applied here are $p_T^b > 40$ GeV, $E_{\cancel{H}} > 100$ GeV.
- Four b-jet with single lepton ($4b\ell$): $4b + \ell + X + E_{\cancel{H}}$; Here X implies any number of inclusive jets without any specific veto on that. The lepton can have any charge \pm . Basic cuts applied here are $p_T^b > 40$ GeV, $p_T^\ell > 20$ GeV, $|\eta| < 2.5$, $E_{\cancel{H}} > 100$ GeV.
- Two b-jets with di-lepton ($2b2\ell$): $2b + 2\ell + X + E_{\cancel{H}}$; Here X implies any number of inclusive jets without any specific veto on that. Leptons can have any charge \pm (including same and opposite sign). Basic cuts applied here are $p_T^b > 40$ GeV, $p_T^\ell > 20$ GeV, $|\eta| < 2.5$, $E_{\cancel{H}} > 100$ GeV.
- Same sign dilepton with inclusive jets ($\ell^\pm\ell^\pm$): $\ell^\pm\ell^\pm + X + E_{\cancel{H}}$; The basic cuts applied are $E_{\cancel{H}} > 30$ GeV, $p_T^{\ell_1} > 40$ GeV and $p_T^{\ell_2} > 30$ GeV with $|\eta| < 2.5$.
- Tripleton with inclusive jets ($\ell^\pm\ell^\pm\ell^\pm$): $\ell^\pm\ell^\pm\ell^\pm + X + E_{\cancel{H}}$; Basic cuts $E_{\cancel{H}} > 30$ GeV, $p_T^{\ell_1} > 30$ GeV, $p_T^{\ell_2} > 30$ GeV and $p_T^{\ell_3} > 20$ GeV with $|\eta| < 2.5$.

- Four-lepton with inclusive jets ($\ell^\pm\ell^\pm\ell^\pm\ell^\pm$): $\ell^\pm\ell^\pm\ell^\pm\ell^\pm + X + E_{\cancel{T}}$; For basic cuts no missing energy cut is employed while, lepton transverse momentum cuts are as follows: $p_T^{\ell_1} > 20$ GeV, $p_T^{\ell_2} > 20$ GeV and $p_T^{\ell_3} > 20$ GeV and $p_T^{\ell_4} > 20$ GeV with $|\eta| < 2.5$.

ℓ stands for final state isolated electrons and or muons as discussed above and $E_{\cancel{T}}$ depicts the missing energy. Opposite-sign dilepton was not considered mainly because of the huge SM background from $t\bar{t}$ process.

Apart from the basic cuts including a Z-veto of $|M_Z - M_{\ell^+\ell^-}| \geq 15$ GeV on same flavor opposite sign dilepton arising in $2b2l$, trilepton and four lepton final states, we apply sum of lepton p_T cut ($\sum p_T^{\ell_i}$) and combination of lepton p_T cut with MET, called modified effective mass cut $H_{T1} = \sum p_T^{\ell_i} + E_{\cancel{T}}$ to the leptonic final states, and harder H_T cuts on b-rich final states and we refer to them as follows:

- $C1$: $\sum p_T^{\ell_i} > 200$ GeV
- $C2$: $\sum p_T^{\ell_i} > 400$ GeV
- $C3$: $H_{T1} > 400$ GeV
- $C4$: $H_{T1} > 500$ GeV
- $C1'$: $\sum p_T^{\ell_i} > 100$ GeV
- $C2'$: $\sum p_T^{\ell_i} > 200$ GeV
- $C3'$: $H_{T1} > 150$ GeV
- $C4'$: $H_{T1} > 250$ GeV
- $C5$: $H_T > 1000$ GeV, $E_{\cancel{T}} > 200$ GeV, $p_T^b > 60$ GeV.

We have generated dominant SM events from $t\bar{t}$ in `Pythia` for the same final states with same cuts and multiplied the corresponding events in different channels by proper K -factor (1.59) to obtain the usually noted next to leading order (NLO) and next to leading log resummed (NLL) cross-section at LHC [48]. $b\bar{b}b\bar{b}$, $b\bar{b}b\bar{b}W/Z$ and $t\bar{t}b\bar{b}$ background have been calculated in `Madgraph5` [49]. The cuts are motivated such that we reduce the background to a great extent as shown in next subsection. Note that softer cuts $C1'$, $C2'$, $C3'$, $C4'$ have been used for four lepton channel where the SM background is much smaller.

| Model Points | Total | $\tilde{g}\tilde{g}$ | $\tilde{t}_1\tilde{t}_1^*$ | $\tilde{\chi}_i^0\tilde{\chi}_j^0$ | $\tilde{\chi}_i^\pm\tilde{\chi}_j^\mp$ | $\tilde{\chi}_i^0\tilde{\chi}_j^\pm$ | $\tilde{g} \rightarrow \tilde{t}_1\bar{t}$ | $\tilde{t}_1 \rightarrow t\chi_1^0$ | $\tilde{t}_1 \rightarrow b\chi_1^+$ |
|--------------|-------|----------------------|----------------------------|------------------------------------|--|--------------------------------------|--|-------------------------------------|-------------------------------------|
| BP1 | 107.6 | 29.20 | 32.06 | 0.11 | 7.18 | 14.6 | 99 % | 76.3 % | 23.7 % |
| BP2 | 607 | 26.3 | 15.1 | 64.7 | 126.9 | 354.8 | 99 % | 10.3% | 45.2% |
| BP3 | 188 | 26.5 | 13.8 | 0.33 | 37.1 | 74.2 | 99 % | 86.5% | 9.4% |
| MSG | 18208 | 39 | 18010 | 0.1 | 28 | 84 | 99% | 0% | 0% |

Table 3: Total supersymmetric particle production cross-sections (in fb) as well as some leading contributions from $\tilde{g}\tilde{g}$ and $\tilde{t}_1\tilde{t}_1^*$ and electroweak neutralino-chargino productions for each of the benchmark points with $E_{CM}=14$ TeV. We also quote the significant decay branching fractions (in percentage).

3.2 Numerical results

The main SUSY production cross-sections for the benchmark points have been noted in Table 3 with the total cross-section for all 2→2 SUSY processes. All the non-universal benchmark points have similar gluino production and third family stop production, while the mSUGRA point has a huge stop production due to very light stop mass and the total cross-section for this point is also dominated by that. Although other benchmark points have sufficiently large branching fraction of stop going to bottom chargino or stop neutralino, MSG has nothing in these channels as the stop is almost degenerate with the lightest neutralino, it only decays to $c\tilde{\chi}_1^0$ in loop. For MSG, $\tilde{\chi}_2^0$ decays to $\tilde{\chi}_1^0 h$ 95% and first chargino dominantly decays to $\tilde{t}_1\bar{b}$. Hence 3b channel can be a better channel to look for such MSG points. As mSUGRA is only alive in such a region of parameter space for the sake of dark matter, all MSG points will be similar in this aspect. We also note that for BP1: $\tilde{\chi}_1^\pm$ decays into $\ell + \nu_\ell + \tilde{\chi}_1^0$ through off-shell sleptons in 33% while $\tilde{\chi}_2^0$ decays to leptonic final state is only $\simeq 1\%$. BP2 has dominant production in electroweak gauginos. Associated production of the gluinos with neutralinos are also quite heavy. Here $\tilde{t}_1 \rightarrow t\tilde{\chi}_{2,3}^0$ branchings are also of the same order of $\tilde{t}_1 \rightarrow t\tilde{\chi}_1^0$. Although $\tilde{\chi}_2^0$ decays to leptonic final state is 1%, $\tilde{\chi}_1^\pm$ decays into $\ell + \nu_\ell + \tilde{\chi}_1^0$ in 33%. Huge electroweak production will significantly contribute to leptonic final states for BP2. For BP3, chargino and neutralino decays to tau-rich final state as a result of lighter stau. Hence, in addition to the standard leptons, channels with tau-tagging can be a better channel to look for this benchmark point.

Missing energy distribution of the benchmark points in bottom rich final states are shown

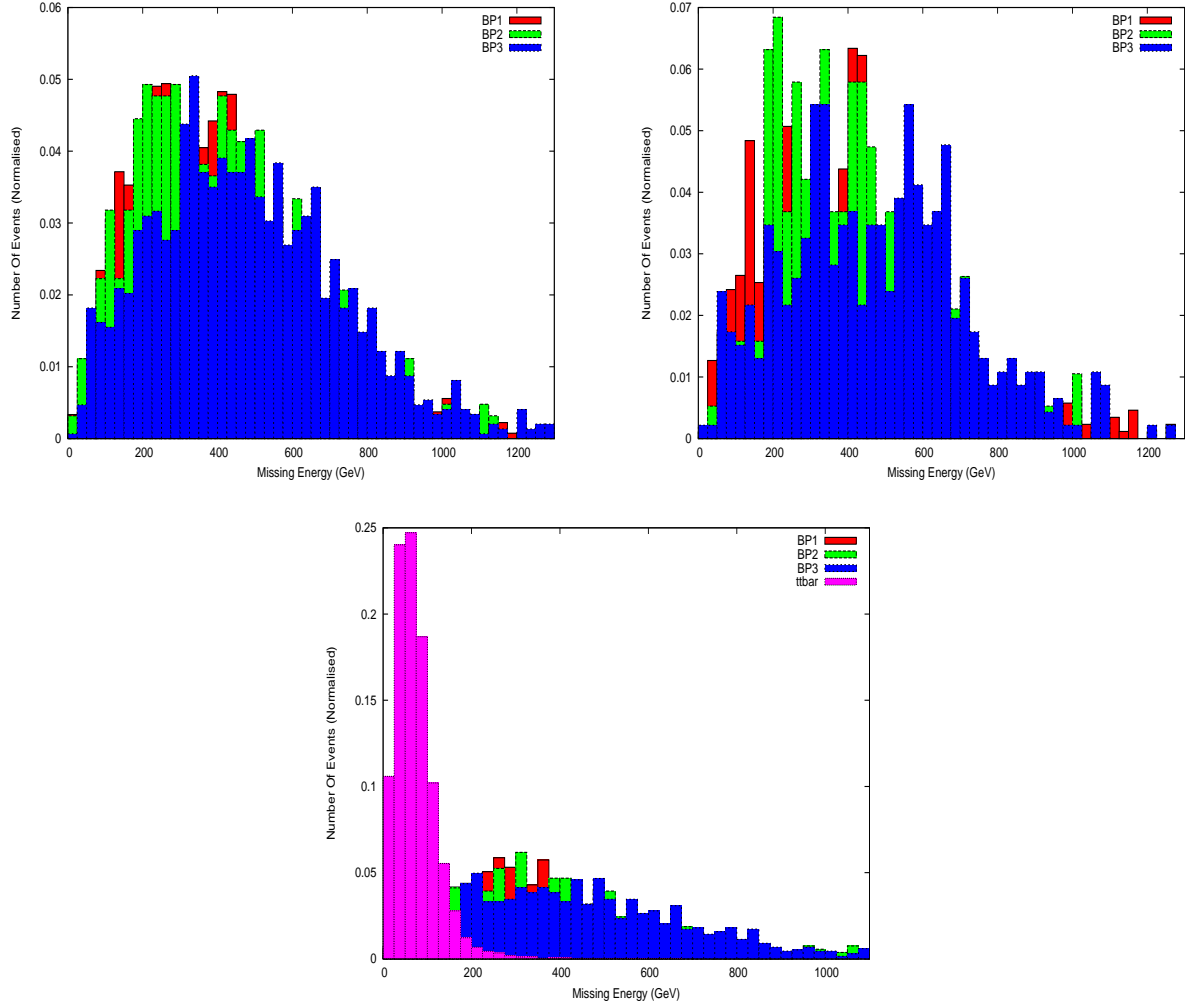


Figure 3: Missing energy distribution in bottom rich final states at the benchmark points. Top left: $4b$ channel, Top right: $4b\ell$ channel; bottom: $2b2\ell$ channel. CTEQ5L pdfset was used. Factorization and Renormalization scale has been set to $\mu_F = \mu_R = \sqrt{\hat{s}}$, sub-process centre of mass energy.

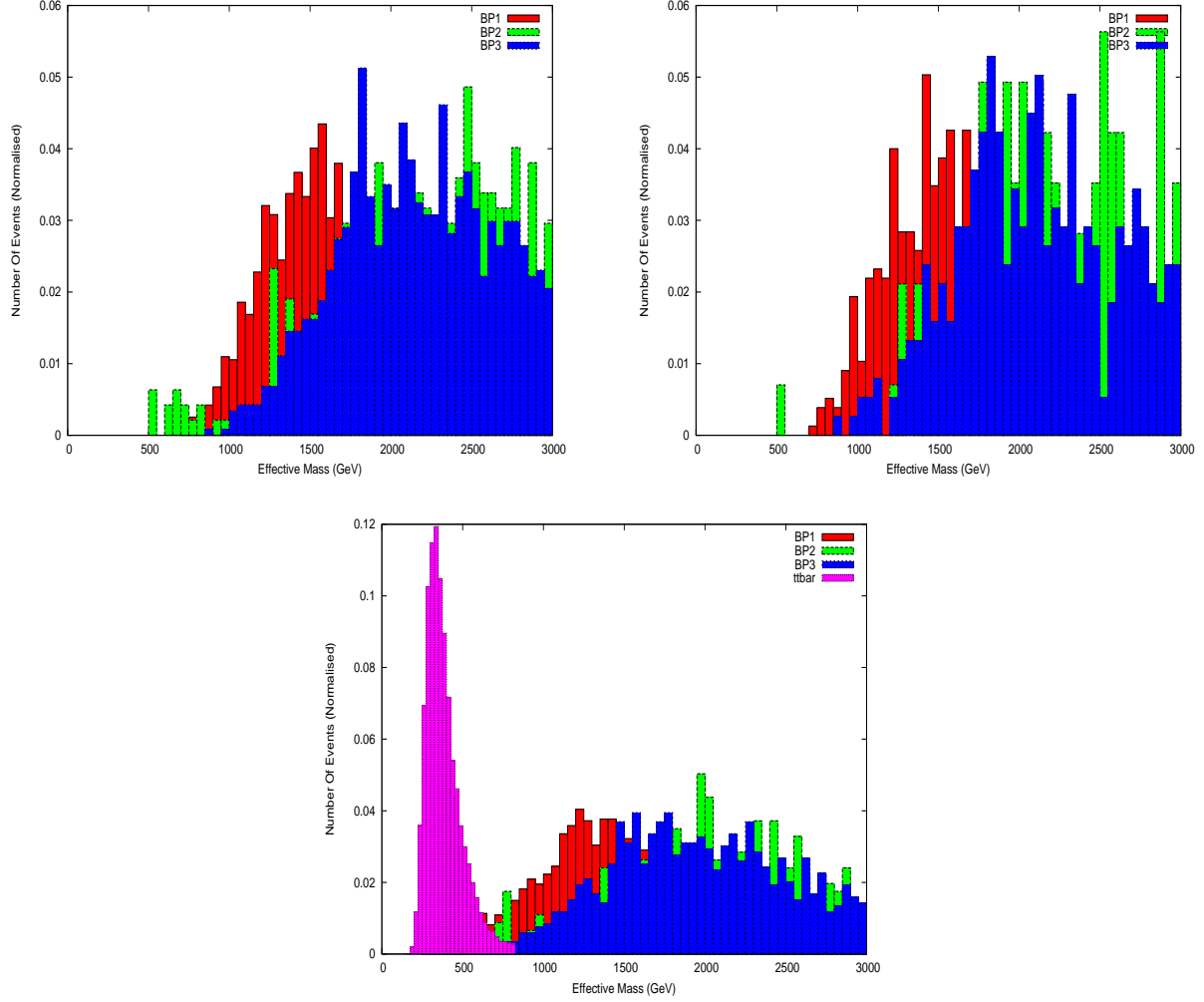


Figure 4: Effective mass distribution in bottom rich final states at the benchmark points. Top left: $4b$ channel, Top right: $4b\ell$ channel; bottom: $2b2\ell$ channel. CTEQ5L pdfset was used. Factorization and Renormalization scale has been set to $\mu_F = \mu_R = \sqrt{\hat{s}}$, sub-process centre of mass energy.

| Benchmark Points | σ_{4b} | σ_{4bl} | σ_{2b2l} | $\sigma_{4b}(C5)$ | $\sigma_{4bl}(C5)$ | $\sigma_{2b2l}(C5)$ |
|--|---------------|----------------|-----------------|-------------------|--------------------|---------------------|
| BP1 | 1.35 | 0.44 | 1.15 | 0.60 | 0.18 | 0.84 |
| BP2 | 1.56 | 0.50 | 1.24 | 1.53 | 0.49 | 1.11 |
| BP3 | 1.34 | 0.41 | 1.17 | 0.76 | 0.22 | 0.91 |
| MSG | 0.004 | 0.004 | 0.1 | ≤ 0.001 | ≤ 0.001 | 0.01 |
| $t\bar{t}$ | ≤ 0.01 | ≤ 0.01 | 973.1 | ≤ 0.01 | ≤ 0.01 | ≤ 0.01 |
| $b\bar{b}b\bar{b}, b\bar{b}b\bar{b} + W/Z$ | 0.106 | ≤ 0.01 | ≤ 0.01 | ≤ 0.01 | ≤ 0.01 | ≤ 0.01 |
| $t\bar{t}b\bar{b}$ | 0.8825 | 0.634 | 1.03 | 0.005 | ≤ 0.01 | ≤ 0.01 |

Table 4: Event-rates (fb) in bottom rich final states at the chosen benchmark points for $E_{CM} = 14$ TeV with basic cuts and cuts $C5$. CTEQ5L pdfset was used. Factorization and Renormalization scale has been set to $\mu_F = \mu_R = \sqrt{\hat{s}}$, subprocess centre of mass energy. Contributions from dominant SM backgrounds are also noted.

in figure 3. Missing Energy has been normalized to 1. $4b$ and $4bl$ final states doesn't have a significant background, hence only signal events are shown. It occurs that the benchmark points have a similar missing energy pattern, while for $2b2l$, the $t\bar{t}$ background has a sharper peak at low missing energy as can be expected. Similarly effective mass H_T distribution in bottom-rich final states is shown in figure 4. There is no significant difference between the benchmark points in terms of this distribution either. We can see for $4bl$ channel (Fig 3, top right), the peaks of the distributions are a bit separated. For $2b2l$, background $t\bar{t}$ peaks at a much lower value while the signal events have a peak ≥ 1000 GeV. This gives us the opportunity to put a very hard effective mass H_T cut, which reduces the background to almost zero, while retaining the signal. Hard effective mass cut also helps to remove other hadronic and QCD backgrounds as shown in Table 4.

In summary, from Table 4, BP1, BP2 and BP3 have very good prospects of being discovered at LHC in $4b$, $4bl$ and $2b2l$ final states while the corresponding MSG point doesn't contribute at all in such final states. The main reason of this is clear from Table 3. Although $\tilde{t}_1\tilde{t}_1^*$ production is huge for MSG, stop being almost degenerate with LSP, it can not decay to $t\tilde{\chi}_1^0$ or $b\tilde{\chi}_1^+$ and hence it doesn't produce any b -jets. We might however, see $3b$ events from electroweak production.

The SM backgrounds are negligible in bottom rich channels excepting $2b2l$, which suffers

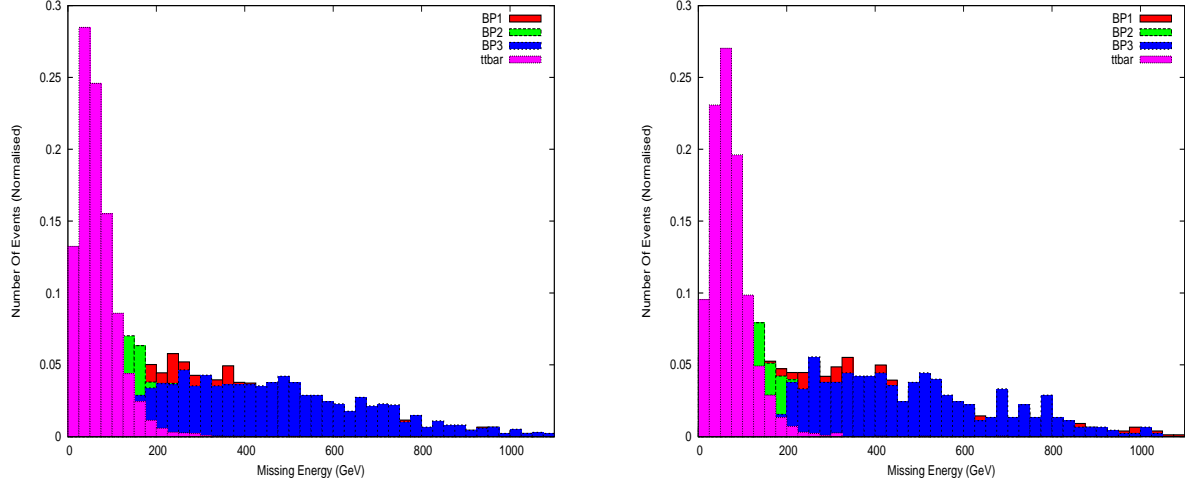


Figure 5: Missing energy distribution in $\ell^\pm\ell^\pm$ (left) and $\ell^\pm\ell^\pm\ell^\pm$ (right) final states at the benchmark points.

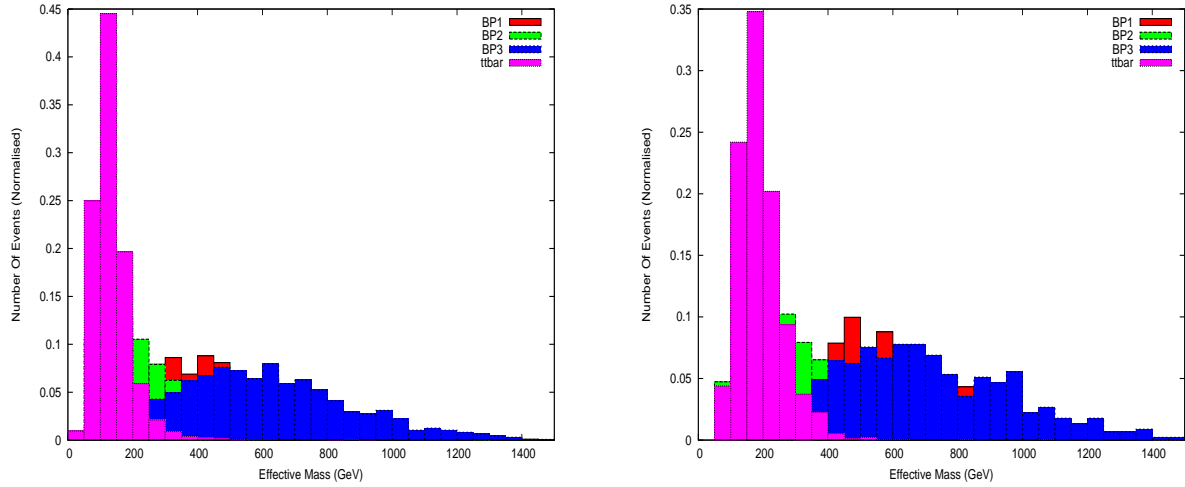


Figure 6: Effective mass H_{T_1} distribution in $\ell^\pm\ell^\pm$ (left) and $\ell^\pm\ell^\pm\ell^\pm$ (right) final states at the benchmark points.

| Channels and Event rates (fb) | BP1 | BP2 | BP3 | MSG | $t\bar{t}$ |
|-----------------------------------|-------|------|-------|--------------|-------------|
| $l^\pm l^\pm$ (Basic) | 0.48 | 1.03 | 0.65 | 0.2 | 40.32 |
| $l^\pm l^\pm + C1$ | 0.16 | 0.30 | 0.30 | 0.1 | 1.08 |
| $l^\pm l^\pm + C2$ | 0.03 | 0.03 | 0.05 | ≤ 0.001 | ≤ 0.01 |
| $l^\pm l^\pm + C3$ | 0.35 | 0.53 | 0.54 | 0.1 | 0.54 |
| $l^\pm l^\pm + C4$ | 0.26 | 0.40 | 0.44 | ≤ 0.001 | 0.17 |
| $l^\pm l^\pm l^\pm$ (Basic) | 0.18 | 0.96 | 0.24 | ≤ 0.001 | 33.96 |
| $l^\pm l^\pm l^\pm + C1$ | 0.11 | 0.40 | 0.18 | ≤ 0.001 | 3.62 |
| $l^\pm l^\pm l^\pm + C2$ | 0.02 | 0.06 | 0.04 | ≤ 0.001 | 0.17 |
| $l^\pm l^\pm l^\pm + C3$ | 0.15 | 0.38 | 0.22 | ≤ 0.001 | 0.54 |
| $l^\pm l^\pm l^\pm + C4$ | 0.11 | 0.31 | 0.19 | ≤ 0.001 | ≤ 0.01 |
| $l^\pm l^\pm l^\pm l^\pm$ (Basic) | 0.018 | 0.21 | 0.019 | ≤ 0.001 | 0.17 |
| $l^\pm l^\pm l^\pm l^\pm + C1'$ | 0.018 | 0.20 | 0.019 | ≤ 0.001 | 0.17 |
| $l^\pm l^\pm l^\pm l^\pm + C2'$ | 0.013 | 0.11 | 0.017 | ≤ 0.001 | ≤ 0.01 |
| $l^\pm l^\pm l^\pm l^\pm + C3'$ | 0.017 | 0.21 | 0.019 | ≤ 0.001 | 0.17 |
| $l^\pm l^\pm l^\pm l^\pm + C4'$ | 0.016 | 0.16 | 0.019 | ≤ 0.001 | ≤ 0.01 |

Table 5: Event-rates (fb) in leptonic final states at the chosen benchmark points for $E_{CM}=14$ TeV with basic cuts and cuts $C1, C2, C3, C4$ as described. The main background $t\bar{t}$ is also noted. CTEQ5L pdfset was used. Factorization and Renormalization scale has been set to $\mu_F = \mu_R = \sqrt{\hat{s}}$, subprocess centre of mass energy. Note that trilepton and four-lepton final states include Z -veto.

from a sufficiently large background from $t\bar{t}$ production. But, a heavy Effective mass cut (H_T) eliminates this to a large extent, while retaining the signals. The Effective mass distribution in Fig. 4 bears the testimony to the fact. We also note that SM background events were simulated with very high number of events, such that each event carries a small weight, 0.01 fb of cross-section; hence, null events in simulation corresponds to cross-section less than that.

Missing energy and effective mass distribution for Same-sign dilepton and trilepton events are shown in fig 5 and 6 respectively. Again all the benchmark points show very similar distribution, while the $t\bar{t}$ can be reduced with a heavy H_{T_1} cut. All the leptonic event numbers for the benchmark points are shown in Table 5.

Table 5 tells us, that trilepton events are still good for all the benchmark points while 4-lepton channel is good for BP2 and BP3 only. We also need to note that the background for 4-lepton channel is negligible (hadronically quiet part comes from $4W$ or ZZZ production). After the cuts they vanish almost completely. Similarly ZW , which contributes to trilepton reduces to a great extent after the Z-veto. Hence, we didn't quote those background events here. We also see that $C2$ and $C4$ cut reduce the $t\bar{t}$ background significantly. $C2$ kills the signal events to a great extent too, hence, $C4$ is a better choice to reduce background and retain signal. Hence, these leptonic final states are also good channels to study such benchmark points. The reason of BP2 having larger leptonic events, comes also from huge electroweak gaugino productions as pointed in Table 3. Hence, a significant part of these leptonic final states should contain hadronically quiet lepton events. The minimal supergravity benchmark point doesn't contribute at all to the leptonic final states, the reason being simply understood as not having lighter stops to decay through top or sleptons leading to leptons. Hence, such mSUGRA points can only be studied in hadronic channels or perhaps $3b$ final states as mentioned earlier. After mSUGRA being alive only in stop co-annihilation region, this seems to be a generic feature for all mSUGRA parameter space points to obey Higgs mass and dark matter constraint. This in turn, can help distinguishing such non-universal frameworks from mSUGRA in LHC signature space.

4 Summary and Conclusions

It is remarkable that a Higgs boson has been discovered with a mass $\simeq 125$ GeV. In pure SM, theoretically there is no reason why its mass should be at the EW scale, or even it is, why it is not much higher or lower than 125 GeV. (In fact, in pure SM, best fit to the EW data prefers a much lower mass). This gives us hope that some symmetry principle is there beyond the pure SM, and supersymmetry being the most natural candidate, because it solves the hierarchy problem, as well as it constraints the Higgs mass to be less than ~ 135 GeV. In addition, supersymmetry has a natural candidate for the dark matter. However, the minimal version of the most desirable version of MSSM, mSUGRA, is in very tight corner to satisfy all the existing experimental constraints, as well as being within the reach of LHC. We find that mSUGRA is still viable in the stop co-annihilation region in which the classic SUSY signal (multijet plus missing E_T) is essentially unobservable beyond the SM background at the LHC. (The other allowed region such as hyperbolic/ focus point has SUSY particle masses well beyond the reach of LHC). However, if we relax little bit from mSUGRA with

non-universal gaugino and /or scalar masses, the situation becomes much more favorable to discover SUSY at the LHC.

In this work, we have shown that SUSY with non-universalities in gaugino or scalar masses within high scale SUGRA set up can still be accessible at LHC with $E_{CM} = 14$ TeV. In particular, we show the consistency of the parameter space in different dark matter annihilation regions. Wino dominated LSP with chargino co-annihilation can be achieved with gaugino mass non-universality with $M_3 < M_2 < M_1$. Hyperbolic Branch/Focus point region with Higgsino dominated LSP can be obtained easily with Higgs non-universality as BP2. Such parameter space automatically occurs with lighter gauginos and hence they may dominate the production and leptonic final states at LHC. Stau co annihilation can occur with scalar non-universality while stop co annihilation can arise simply with high-scale gaugino non-universality with $M_3 < M_2 = M_1$. mSUGRA, though viable in only stop co-annihilation region, do not yield lepton or b-rich final states due to lack of phase space for the stop to decay leptonically. There exist a reasonable region of parameter space in the non-universal scenario which not only satisfy all the existing constraints, but also can unravel SUSY in bottom and lepton rich final states with third family squarks being lighter than the first two automatically. We have made detailed studied of three benchmark points in these allowed parameter spaces, and find that SUSY signal in the bottom or bottom plus lepton-rich final state stands over the SM background with suitable cuts. We have also investigated pure leptonic final states with suitable cuts, and find some of these final state have viable prospects. Finally we also emphasize that with good luminosity in the upcoming 14 TeV LHC runs, these allowed parameter space can be ruled out easily, or we we will discover SUSY.

Acknowledgment: The work of SB is supported by the U.S. Department of Energy under Grant No. DE-SC0008541. The work of SC, KG and SN was supported in part by the U.S. Department of Energy Grant Number DE-SC0010108.

References

- [1] For reviews on Supersymmetry, see, e.g., H. P. Nilles, Phys. Rep. **1**, 110 (1984); H. E. Haber and G. Kane, Phys. Rep. **117**, 75 (1985) ; J. Wess and J. Bagger, *Supersymmetry and Supergravity*, 2nd ed., (Princeton, 1991); H. Baer and X. Tata, *Weak Scale Supersymmetry*, Cambridge University Press, 2006; M. Drees, R. Godbole

and P. Roy, *Hackensack, USA: World Scientific (2004) 555 p*; P. Binetruy, *Oxford, UK: Oxford Univ. Pr. (2006) 520 p*.

- [2] D. J. H. Chung et al., *Phys. Rept.* **407**, 1 (2005); S. P. Martin, arXiv:hep-ph/9709356.
- [3] A. H. Chamseddine, R. Arnowitt and P. Nath, *Phys. Rev. Lett.* **49**, 970 (1982); R. Barbieri, S. Ferrara and C. A. Savoy, *Phys. Lett. B* **119**, 343 (1982); L. J. Hall, J. Lykken and S. Weinberg, *Phys. Rev. D* **27**, 2359 (1983); P. Nath, R. Arnowitt and A. H. Chamseddine, *Nucl. Phys. B* **227**, 121 (1983); N. Ohta, *Prog. Theor. Phys.* **70**, 542 (1983).
- [4] G. Aad *et al.* [ATLAS Collaboration], *Phys. Rev. Lett.* **106**, 131802 (2011) [arXiv:1102.2357 [hep-ex]]; G. Aad *et al.* [ATLAS Collaboration], *Phys. Rev. D* **85**, 012006 (2012) [arXiv:1109.6606 [hep-ex]]; G. Aad *et al.* [ATLAS Collaboration], *Phys. Lett. B* **709**, 137 (2012) [arXiv:1110.6189 [hep-ex]]; G. Aad *et al.* [ATLAS Collaboration], *Phys. Rev. Lett.* **108**, 261804 (2012) [arXiv:1204.5638 [hep-ex]]; G. Aad *et al.* [ATLAS Collaboration], *Phys. Rev. D* **86**, 092002 (2012) [arXiv:1208.4688 [hep-ex]]; G. Aad *et al.* [ATLAS Collaboration], [ATLAS Collaboration], ATLAS-CONF-2012-105; S. Chatrchyan *et al.* [CMS Collaboration], *Phys. Rev. Lett.* **106**, 211802 (2011) [arXiv:1103.0953 [hep-ex]].
- [5] G. Aad *et al.* [ATLAS Collaboration], *Phys. Rev. D* **85**, 112006 (2012) [arXiv:1203.6193 [hep-ex]].
- [6] S. Chen, et al., CLEO Collaboration, *Phys. Rev. Lett.* **87**, 251807 (2001), hep-ex/0108032; P. Koppenburg *et al.* [Belle Collaboration], *Phys. Rev. Lett.* **93**, 061803 (2004) B. Aubert, et al., BaBar Collaboration, hep-ex/0207076.
- [7] RAaib *et al.* [LHCb Collaboration], *Phys. Rev. Lett.* **110**, 021801 (2013).
- [8] V. D. Barger, C. Kao and R. J. Zhang, *Phys. Lett. B* **483** (2000) 184 [arXiv:hep-ph/9911510].
- [9] Y. Nir and N. Seiberg, *Phys. Lett. B* **309** (1993) 337 [arXiv:hep-ph/9304307]; M. Dine, A. E. Nelson and Y. Shirman, *Phys. Rev. D* **51** (1995) 1362 [arXiv:hep-ph/9408384]; L. Randall and R. Sundrum, *Nucl. Phys. B* **557** (1999) 79 [arXiv:hep-th/9810155].
- [10] N. Desai and B. Mukhopadhyaya, *Phys. Rev. D* **80**, 055019 (2009) [arXiv:0901.4883 [hep-ph]]; H. Baer, V. Barger, A. Lessa and X. Tata, *JHEP* **1006**, 102 (2010)

- [arXiv:1004.3594 [hep-ph]]; M. A. Ajaib, T. Li, Q. Shafi and K. Wang, arXiv:1011.5518 [hep-ph]; S. Bornhauser, M. Drees, S. Grab and J. S. Kim, arXiv:1011.5508 [hep-ph]; N. Chen, D. Feldman, Z. Liu, P. Nath and G. Peim, arXiv:1011.1246 [hep-ph]; N. Chen, D. Feldman, Z. Liu, P. Nath and G. Peim, arXiv:1010.0939 [hep-ph].
- [11] U. Chattopadhyay and D. Das, Phys. Rev. D **79**, 035007 (2009) [arXiv:0809.4065 [hep-ph]]; S. Bhattacharya, U. Chattopadhyay, D. Choudhury, D. Das and B. Mukhopadhyaya, Phys. Rev. D **81**, 075009 (2010) [arXiv:0907.3428 [hep-ph]].
- [12] V. Berezhinsky, A. Bottino, J. R. Ellis, N. Fornengo, G. Mignola and S. Scopel, Astropart. Phys. **5**, 1 (1996) [hep-ph/9508249].
- [13] P. Nath and R. Arnowitt, Phys. Rev. D **56**, 2820 (1997); D. Feldman, Z. Liu and P. Nath, JHEP **0804**, 054 (2008); D. Feldman, Z. Liu and P. Nath, Phys. Rev. D **78**, 083523 (2008).
- [14] D. G. Cerdeno and C. Munoz, JHEP **0410**, 015 (2004) [arXiv:hep-ph/0405057].
- [15] J. Ellis, K. A. Olive and P. Sandick, arXiv:0805.2343 [hep-ph]; J. R. Ellis, K. A. Olive, Y. Santoso and V. C. Spanos, Phys. Lett. B **603**, 51 (2004); J. R. Ellis, T. Falk, K. A. Olive and Y. Santoso, Nucl. Phys. B **652**, 259 (2003) [arXiv:hep-ph/0210205]; A. De Roeck et al., Y , J. R. Ellis, F. Gianotti, F. Moortgat, K. A. Olive and L. Pape, Eur. Phys. J. C **49**, 1041 (2007) [arXiv:hep-ph/0508198].
- [16] H. Baer, A. Mustafayev, E. K. Park and X. Tata, JHEP **0805**, 058 (2008); H. Baer et al., JHEP **0604**, 041 (2006).
- [17] Y. Kawamura, H. Murayama and M. Yamaguchi, Phys. Rev. D **51** (1995) 1337 [arXiv:hep-ph/9406245]; Y. Kawamura, H. Murayama and M. Yamaguchi, Phys. Lett. B **324** (1994) 52 [arXiv:hep-ph/9402254].
- [18] A. Datta, A. Datta, M. Drees and D. P. Roy, Phys. Rev. D **61**, 055003 (2000) [arXiv:hep-ph/9907444]; A. Datta, A. Datta and M. K. Parida, Phys. Lett. B **431**, 347 (1998) [arXiv:hep-ph/9801242].
- [19] S. Bhattacharya, A. Datta and B. Mukhopadhyaya, Phys. Rev. D **78**, 035011 (2008) [arXiv:0804.4051 [hep-ph]]; B. S. Acharya, P. Grajek, G. L. Kane, E. Kuffik, K. Suruliz and L. T. Wang, arXiv:0901.3367 [hep-ph].

- [20] J. R. Ellis, C. Kounnas and D. V. Nanopoulos, Nucl. Phys. B **247**, 373 (1984); J. R. Ellis, K. Enqvist, D. V. Nanopoulos and K. Tamvakis, Phys. Lett. B **155**, 381 (1985); M. Drees, Phys. Lett. B **158**, 409 (1985); A. Corsetti and P. Nath, Phys. Rev. D **64**, 125010 (2001) [arXiv:hep-ph/0003186]; A. Corsetti and P. Nath, Phys. Rev. D **64**, 125010 (2001); U. Chattopadhyay, A. Corsetti and P. Nath, Phys. Rev. D **66**, 035003 (2002); N. Chamoun, C. S. Huang, C. Liu and X. H. Wu, Nucl. Phys. B **624**, 81 (2002) [arXiv:hep-ph/0110332]; U. Chattopadhyay and D. P. Roy, Phys. Rev. D **68**, 033010 (2003); U. Chattopadhyay, D. Choudhury and D. Das, Phys. Rev. D **72**, 095015 (2005); R. C. Cotta, J. S. Gainer, J. L. Hewett and T. G. Rizzo, Nucl. Phys. Proc. Suppl. **194**, 133 (2009) [arXiv:0909.4088 [hep-ph]]; J. Chakraborty and A. Raychaudhuri, Phys. Lett. B **673** (2009) 57 [arXiv:0812.2783 [hep-ph]].
- [21] S. Bhattacharya, A. Datta and B. Mukhopadhyaya, JHEP **0710**, 080 (2007) [arXiv:0708.2427 [hep-ph]]; S. Bhattacharya, A. Datta and B. Mukhopadhyaya, Phys. Rev. D **78**, 115018 (2008) [arXiv:0809.2012 [hep-ph]]; S. P. Martin, Phys. Rev. D **79**, 095019 (2009) [arXiv:0903.3568 [hep-ph]]; S. Bhattacharya and J. Chakraborty, Phys. Rev. D **81**, 015007 (2010) [arXiv:0903.4196 [hep-ph]].
- [22] S. Bhattacharya and S. Nandi, arXiv:1101.3301 [hep-ph].
- [23] G. Aad *et al.* [ATLAS Collaboration], Phys. Lett. B **716**, 1 (2012) [arXiv:1207.7214 [hep-ex]]; S. Chatrchyan *et al.* [CMS Collaboration], Phys. Lett. B **716**, 30 (2012) [arXiv:1207.7235 [hep-ex]].
- [24] E. Komatsu *et al.* [WMAP Collaboration], arXiv:0803.0547 [astro-ph].
- [25] P. A. R. Ade *et al.* [Planck Collaboration], arXiv:1303.5076 [astro-ph.CO].
- [26] X. -J. Bi, Q. -S. Yan and P. -F. Yin, Phys. Rev. D **85**, 035005 (2012); S. Bornhauser, M. Drees, S. Grab and J. S. Kim, Phys. Rev. D **83**, 035008 (2011); K. Ghosh, K. Huitu, J. Laamanen, L. Leinonen, Phys. Rev. Lett. **110**, 141801 (2013); M. Carena, A. Freitas and C. E. M. Wagner, JHEP **0810**, 109 (2008); M. Drees, M. Hanussek and J. S. Kim, Phys. Rev. D **86**, 035024 (2012).
- [27] H. Baer, V. Barger, P. Huang, D. Mickelson, A. Mustafayev and X. Tata, Phys. Rev. D **87** (2013) 035017; Sujit Akula and Pran Nath, arXiv:1304.5526; M. Kahl-Rowley, J. L. Hewett, A. Ismail and T. G. Rizzo, arXiv:1307.8444; Taoli Cheng and Tianjun Li, arXiv:1305.3214; Ilia Gogoladze, Fariha Nasir and Qaisar Shafi,

- arXiv:1212.2593; S. Caron, J. Laamanen and A. Strubig, JHEP 1206 (2012)008; Marcin Badziak, Marek Olechowski, and Stephan Pokorski, arXiv:1307.7999; A. Spies and G. Anton, arXiv:1306.1099; Nobuchika Okada, shabbar Raza and Qaisar Shafi, arXiv:1107.0941; alexandre Arbeya, Marco Battagliad, Abdelhak and Faravah Mahmoudi, arXiv1211.4004.
- [28] H. Baer and M. Brhlik, Phys. Rev. D **53**, 597 (1996); V. D. Barger and C. Kao, Phys. Rev. D **57**, 3131 (1998).
- [29] http://lepsusy.web.cern.ch/lepsusy/www/sleptons_summer04/slep_final.html
- [30] R. Arnowitt and P. Nath, Phys. Rev. Lett. **70**, 3696 (1993); A. Djouadi, M. Drees and J. Kneur, Phys. Lett. B **624**, 60 (2005).
- [31] M. Drees and M. Nojiri, Phys. Rev. D **47**, 376 (1993); H. Baer and M. Brhlik, Phys. Rev. D **57**, 567 (1998); H. Baer, M. Brhlik, M. Diaz, J. Ferrandis, P. Mercadante, P. Quintana and X. Tata, Phys. Rev. D **63**, 015007 (2001); J. Ellis, T. Falk, G. Ganis, K. Olive and M. Srednicki, Phys. Lett. B **510**, 236 (2001); L. Roszkowski, R. Ruiz de Austri and T. Nihei, JHEP **0108**, 024 (2001); A. Djouadi, M. Drees and J. L. Kneur, JHEP **0108**, 055 (2001); A. Lahanas and V. Spanos, EPJC **23**, 185 (2002).
- [32] K. L. Chan, U. Chattopadhyay and P. Nath, Phys. Rev. D **58**, 096004 (1998); J. Feng, K. Matchev and T. Moroi, Phys. Rev. Lett. **84**, 2322 (2000) and Phys. Rev. D **61**, 075005 (2000); see also H. Baer, C. H. Chen, F. Paige and X. Tata, Phys. Rev. D **52**, 2746 (1995) and Phys. Rev. D **53**, 6241 (1996); H. Baer, C. H. Chen, M. Drees, F. Paige and X. Tata, Phys. Rev. D **59**, 055014 (1999); for a model-independent approach, see H. Baer, T. Krupovnickas, S. Profumo and P. Ullio, JHEP **0510**, 020 (2005).
- [33] J. Ellis, T. Falk and K. Olive, Phys. Lett. B **444**, 367 (1998); J. Ellis, T. Falk, K. Olive and M. Srednicki, Astropart. Phys. **13**, 181 (2000); M.E. Gómez, G. Lazarides and C. Pallis, Phys. Rev. D **61**, 123512 (2000) and Phys. Lett. B **487**, 313 (2000); A. Lahanas, D. V. Nanopoulos and V. Spanos, Phys. Rev. D **62**, 023515 (2000); R. Arnowitt, B. Dutta and Y. Santoso, Nucl. Phys. B **606**, 59 (2001).
- [34] C. Böhm, A. Djouadi and M. Drees, Phys. Rev. D **30**, 035012 (2000); J. R. Ellis, K. A. Olive and Y. Santoso, Astropart. Phys. **18**, 395 (2003); J. Edsjö, *et al.*, JCAP **0304** (2003) 001.
- [35] ATLAS-CONF-2013-047.

- [36] CMS-PAS-SUS-12-028.
- [37] H. Baer, V. Barger and A. Mustafayev, Phys. Rev. D **85**, 075010 (2012) [arXiv:1112.3017 [hep-ph]].
- [38] S. Akula, D. Feldman, Z. Liu, P. Nath and G. Peim, Mod. Phys. Lett. A **26** (2011) 1521 [arXiv:1103.5061]; N. Bhattacharyya, A. Choudhury and A. Datta, Phys. Rev. D **84**, 095006 (2011) [arXiv:1107.1997]; A. Arbey, M. Battaglia and F. Mahmoudi, Eur.Phys.J. C **72** (2012) 1847 [arXiv:1110.3726]; K. A. Olive, [arXiv:1202.2324]; A. J. Williams, C. Boehm, S. M. West and D. A. Vasquez, Phys. Rev. D **86**, 055018 (2012) [arXiv:1204.3727]; A. Arbey, M. Battaglia and F. Mahmoudi, Eur.Phys.J. C **72** (2012) 2169 [arXiv:1205.2557]; W. Wang, Adv.High Energy Phys. **2012** (2012) 216941 [arXiv:1205.5081]; G. Belanger, S. Biswas, C. Boehm and B. Mukhopadhyaya JHEP **12** (2012) 076 [arXiv:1206.5404]; P. Nath, [arXiv:1207.5501]; C. Boehm, P. S. B. Dev, A. Mazumdar and E. Pukartas, [arXiv:1303.5386]; S. Scopel, N. Fornengo and A. Bottino, [arXiv:1304.5353].
- [39] S. Akula, et al., Phys. Rev. D **85**, 075001 (2012) [arXiv:1112.3645]; D. Ghosh, M. Guchait, S. Raychaudhuri and D. Sengupta, Phys. Rev. D **86**, 055007 (2012) [arXiv:1205.2283]; A. Fowlie, et al., Phys. Rev. D **86**, 075010 (2012) [arXiv:1206.0264]; M. Cannoni, O. Panella, M. Pioppi and M. Santoni, Phys. Rev. D **86**, 037702 (2012) [arXiv:1206.5759]; O. Buchmueller, et al., Eur. Phys. J. C **72** (2012) 2243 [arXiv:1207.7315]; G. Arcadi, R. Catena and P. Ullio, [arXiv:1211.5129].
- [40] A. Choudhury and A. Datta, JHEP **1206**, 006 (2012) [arXiv:1203.4106 [hep-ph]]; A. Choudhury and A. Datta, arXiv:1305.0928 [hep-ph].
- [41] See for example, A. Birkedal-Hansen and B. D. Nelson, Phys. Rev. D **64**, 015008 (2001) [hep-ph/0102075]; H. Baer, A. Mustafayev, E. -K. Park and S. Profumo, JHEP **0507**, 046 (2005) [hep-ph/0505227].
- [42] A. Djouadi, J. L. Kneur and G. Moultaka, arXiv:hep-ph/0211331.
- [43] G. Belanger, F. Boudjema, A. Pukhov and A. Semenov, arXiv:1305.0237 [hep-ph].
- [44] T. Sjostrand, S. Mrenna and P. Skands, JHEP **0605**, 026 (2006) [arXiv:hep-ph/0603175].
- [45] P. Skands *et al.*, JHEP **0407**, 036 (2004) [arXiv:hep-ph/0311123].

- [46] H. L. Lai *et al.* [CTEQ Collaboration], *Eur. Phys. J. C* **12**, 375 (2000) [arXiv:hep-ph/9903282].
- [47] ATLAS detector and physics performance. Technical design report. Vol. 2, CERN-LHCC-99-15, ATLAS-TDR-15.
- [48] S. Moch and P. Uwer, “Theoretical status and prospects for top-quark pair production at hadron colliders,” *Phys. Rev. D* **78** (2008) 034003 [arXiv:0804.1476 [hep-ph]].
- [49] J. Alwall, M. Herquet, F. Maltoni, O. Mattelaer and T. Stelzer, *JHEP* **1106**, 128 (2011) [arXiv:1106.0522 [hep-ph]].